New Ku-Band Geophysical Model Function and Wind Speed Retrieval Algorithm Developed for Tiangong-2 Interferometric Imaging Radar Altimeter

Guo Li, Yunhua Zhang, *Member, IEEE*, and Xiao Dong, *Member, IEEE*

***Abstract*—A Ku-band geophysical model function for wind speed retrieval named as KuLMOD-H is proposed based on the quasi-specular reflection model for the Chinese Tiangong-2 Interferometric Imaging Radar Altimeter (TG2-InIRA), which can be used to retrieve the wind speed with 2 km resolution. The model is derived by expanding the effective nadir reflection coefficient term and the mean square slope term in the quasi-specular reflection model using quadratic polynomials with wind speed as variable. The model coefficients are obtained by fitting the radar backscattering coefficient data from TG2-InIRA to the collocated sea surface wind speed data from European Center for Medium-Range Weather Forecasts (ECMWF). For solving the problem of potential ambiguous solutions when the incidence angles are relatively large, a regularization approach is further proposed. The retrieved wind speed results have a root-mean-square error (RMSE) of 1.42 m/s compared with the collocated ECMWF wind speed data and at the same time, they are highly consistent with the buoy data. Different from the previous works on TG2-InIRA wind speed retrieval, this article derives a semiphysical model suitable for incidence angles from 1° to 8°, by which better retrieval results are achieved. This work not only explores the wind speed retrieval capability of the instrument under low incidence-angle observation, but also provides high-resolution wind speed data for further correction of sea state bias for TG2-InIRA sea surface height measurements.**

***Index Terms*—Low incidence angles, quasi-specular reflection, regularization approach, Tiangong-2 interferometric imaging radar altimeter (TG2-InIRA), wind speed retrieval model.**

I. Introduction

THE spaceborne interferometric imaging radar altimeter (TG2-InIRA) was launched onboard the Chinese Tiangong-2 space laboratory on September 15, 2016 [1]. TG2-InIRA works at 13.58 GHz with 40 MHz bandwidth, it is the first wide-swath ocean altimeter [2]. TG2-InIRA aims to validate the working principle for realizing wide-swath measurement of sea surface height (SSH) and the payload design as well [3]–[5]. Different from traditional altimeters, TG2-InIRA takes a short interferometric baseline and adopts small incidence angles from 1° to 8° along with synthetic aperture imaging technique to obtain amplitude images and wide-swath SSH at the same time. Synthetic aperture processing is applied to improving the azimuthal resolution while pulse compression is used to obtain high range resolution under off-nadir observation geometry [6]. Hence, TG2-InIRA can measure SSH with wide-swath and the sea surface normalized backscattering cross section (σ_0) with high resolution owning to the realized high signal to noise ratio (SNR) under the specific observation geometry.

The sea surface wind field is the main power source of the upper ocean motion, which is directly related to almost all the seawater movements in the ocean. Wind speed is one of the important physical parameters in oceanography, which is of great significance for marine environment numerical prediction, marine disaster monitoring, air-sea interaction, meteorological forecast, climate research, etc [7], [8]. Spaceborne remote sensing technologies have been widely used to monitor the sea surface wind field [7], [9], [10]. Geophysical model functions (GMFs), such as the C-band models CMOD4, CMOD5, and the Ku-band models NSCAT-2, Ku-2011, and QSCAT-1 [11]–[17], describe the relationship between σ_0 and incidence angle, polarization, wind speed, and other parameters. They play an important role in retrieving wind field by scatterometer. In fact, GMFs have been also proved to be applicable to the sea surface wind field measurement by synthetic aperture radar (SAR) [18]–[20].

Since the launch of Tropical Rainfall Measuring Mission Precipitation Radar (TRMM PR), the sensitivities of σ_0 at incidence angles less than 20° to winds and waves have been investigated extensively [21]–[26], so as to obtain the relationship between σ_0 and significant wave height (SWH), wind speed and other sea state parameters. It has been shown that σ_0 decreases monotonically as wind speed increases when the incidence angles are from nadir to 5°, while it increases monotonically when the angles are greater than 10°. Besides, σ_0 exhibits low sensitivity to wind speed in the range of 5°–10° [23]. Chu *et al.* [26] analyzed the relationship between σ_0 and wind and wave parameters using collocated National Data Buoy Center (NDBC) buoy data, and found that the sea surface roughness is strongly correlated with wind speed and surface wave slopes. And the sensitivity of σ_0

Manuscript received October 24, 2021; revised January 9, 2022; accepted February 6, 2022. Date of publication February 11, 2022; date of current version March 2, 2022. This work was supported in part by the Marine S&T Fund of Shandong Province for Pilot National Laboratory for Marine Science and Technology (Qingdao) under Grant 2018SDKJ0102-7 and in part by the National Key R&D Program of China under Grant 2016YFC1401004, along with China Manned Space Program. *(Corresponding author: Yunhua Zhang.)*

The authors are with the CAS Key Laboratory of Microwave Remote Sensing, National Space Science Center, Chinese Academy of Sciences, Beijing 100190, China, and also with the School of Electronic, Electrical, and Communication Engineering, University of Chinese Academy of Sciences, Beijing 100049, China (e-mail: liguo17@mails.ucas.ac.cn; zhangyunhua@mirslab.cn; dongxiao@mirslab.cn).

Digital Object Identifier 10.1109/JSTARS.2022.3150390

to wind direction is significantly weaker than to wind speed for incidence angles less than 10°. Accordingly, some wind speed models have been developed. Freilich and Vanhoff constructed an empirical model using PR σ_0 and wind speeds extracted from TRMM Microwave Imager [21]. In 2004, Li *et al.* [27] retrieved the sea surface wind speed from PR measurements using the SASS-2 model function. Bao *et al.* [28] established an empirical GMF to retrieve wind speed using PR σ_0 and QuikScat wind speed data. An artificial neural network model was developed using PR measurements in [29].

As for the interferometric imaging altimeter, Zhang *et al.* [30] retrieved the sea surface wind speed via the neural network approach using TG2-InIRA data. Ren *et al.* upgraded the empirical Ku-band low incidence model (KuLMOD) derived from TRMM PR σ_0 data to KuLMOD2 and applied it to retrieve the wind speed using TG2-InIRA data [3], [31]. The previous works have demonstrated the wind speed measurement ability of TG2-InIRA with good wind speed retrieval results achieved. This work further analyzes the relationship between TG2-InIRA data and sea state parameters at low incidence angles based on the complete data obtained during the whole lifetime, and the data are fully utilized to derive the updated model. Besides, the sea state bias (SSB) of altimeter SSH measurement depending on wind speed and SWH has been widely investigated [32], [33]. Accurate acquisition of wind speed will be helpful for correcting SSB and improving the accuracy of SSH measurement for TG2-InIRA.

This article focuses on wind speed retrieval from TG2-InIRA data and develops a Ku-band high-resolution GMF at low incidence angles (KuLMOD-H) by fitting the measured σ_0 from TG2-InIRA to the model using the wind speed data from European Center for Medium-Range Weather Forecasts (ECMWF). TG2-InIRA σ_0 data used in this work cover a wider range of incidence angles (1°- 8°) than previous works after an updated calibration was performed. We first analyze the relationship between the sea state parameters and σ_0 at low incidence angles and then develop the model based on quasi-specular reflection with the effective nadir reflection coefficient and the mean square slope parameters expanded as quadratic functions of wind speed. To deal with the multivalue ambiguous problem of wind speed retrieval when incidence angles are larger than 4°, a regularization method is proposed. Based on the KuLMOD-H model, the retrieved wind speeds by combining the look-up table approach and the regularization approach are highly consistent with both the reanalysis wind speed data and the buoy data.

The rest of this article is organized as follows. Descriptions of the datasets and the proposed GMF are presented in Sections II and III, respectively. Sections IV and V introduce the wind speed retrieval method and compare the results with that of buoys, reanalysis data, and the existing model. Finally, Section VI concludes this article.

II. Datasets Description

A. TG2-InIRA Observations

A total of 40 tracks of TG2-InIRA data are allocated, among which 21 tracks are matched with the reanalysis data for model establishment and validation, while the remaining 19 tracks are matched with Buoys for model validation. They were acquired between December 2016 and November 2018. The spatial distribution of the tracks is presented in Fig. 1. The raw spatial resolutions of intensity image are about 30 m along-track and 30–300 m cross-track and the ground swath is greater than 40 km. Fig. 2(a) and (b) present TG2-InIRA amplitude images with spatial resolutions of 500 m and 2 km, and they are obtained by performing spatial filtering on the same raw image with 500 m and 2 km windows, respectively. The sea surface σ_0 data contaminated by rainfalls are first screened out before the following processing. The spatial resolution of σ_0 is downgraded to 2 km for guaranteeing much higher SNR, which helps for accurately analyzing their variation versus different incidence angles and different SWHs.

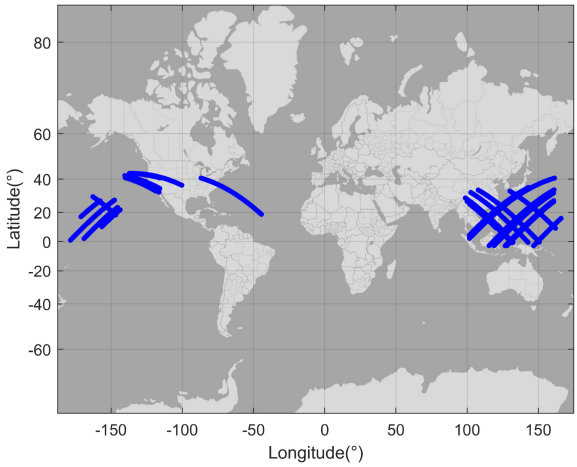

Fig. 1. Spatial coverage of TG2-InIRA data for this study. The data corresponding to less than 50 m depth have been removed out for getting rid of the coastal effects on the measurement.

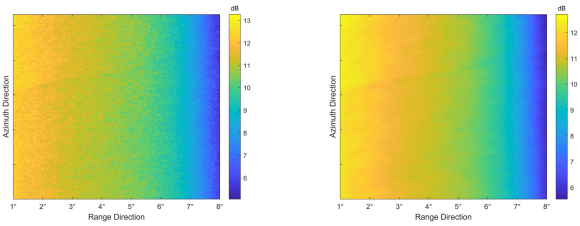

Fig. 2. Amplitude images of TG2-InIRA with resolutions of (a) 500 m and (b) 2 km.

B. ECMWF ERA-5 Data

The wind speed data 10 m above sea surface with 0.25° × 0.25° spatial resolution and 1-h temporal resolution from ECMWF ERA-5 are collocated to match TG2-InIRA data for fitting the model coefficients and validating the developed model. The ECMWF SWH data are also collocated to TG2-InIRA data for analyzing their correlation. The spatial resolution of SWH is 0.5° × 0.5° and the temporal resolution is also 1 h. By using a combined 10-min time window and 2-km spatial

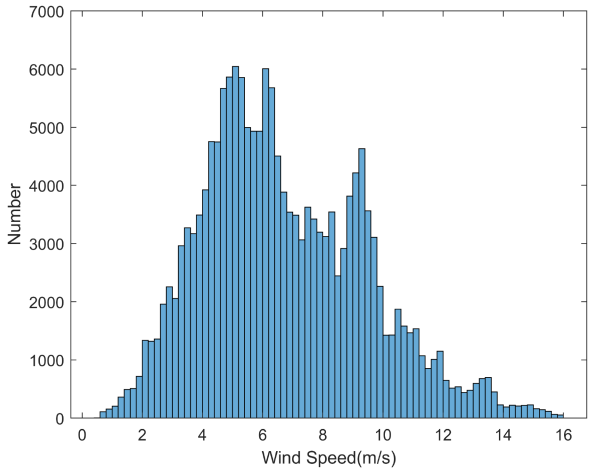

Fig. 3. Histogram of wind speeds from ECMWF matching to TG2-InIRA data.

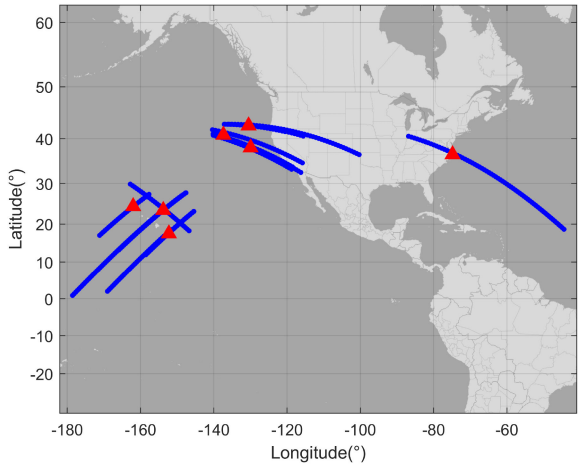

Fig. 4. Spatial distribution of buoys matching to the TG2-InIRA tracks. The red triangles represent the position of the buoys, and the blue lines indicate the tracks of TG2-InIRA.

window, 171 764 groups of ERA-5 data are matched to the TG2-InIRA data. Fig. 3 presents the histogram of the collocated wind speeds, as can be seen from which there is a small number of wind speeds higher than 14 m/s and lower than 2 m/s. The mean and the standard deviation of the collocated wind speeds are, respectively, 6.82 and 2.95 m/s. We randomly select 3/4 of the data for model fitting and the remaining 1/4 of the data for model validation.

C. ETOPO1 Data

The ETOPO1 is built from the global and regional datasets. It is a 1 arc-min global relief model of the Earth's surface integrating both the land topography and the ocean bathymetry. Here, it is used to remove out the shallow water areas with depth less than 50 m.

D. NDBC Buoys Data

The wind speeds from NDBC buoys 50 km away from offshore are used to validate the retrieved wind speeds. The wind speed and wind direction are available per 10 min by buoys, so the time and spatial matching windows of 10 min and 50 km are applied for selecting the data. The spatial distribution of the collocated buoys is presented in Fig. 4, as it is shown, a total of seven NDBC buoys are matched to the TG2-InIRA orbits.

Since the anemometers installed on NDBC buoys are about 3–9 m above the sea surface, so the measured wind speeds are transferred to that of 10 m above sea surface according to the following equation [34]:

$$u = 8.7403 \times \frac{u_z}{\ln \frac{z}{0.0016}} \tag{1}$$

where z represents the height above sea surface, u and u_z represent the wind speed at 10 m and that at z height, respectively.

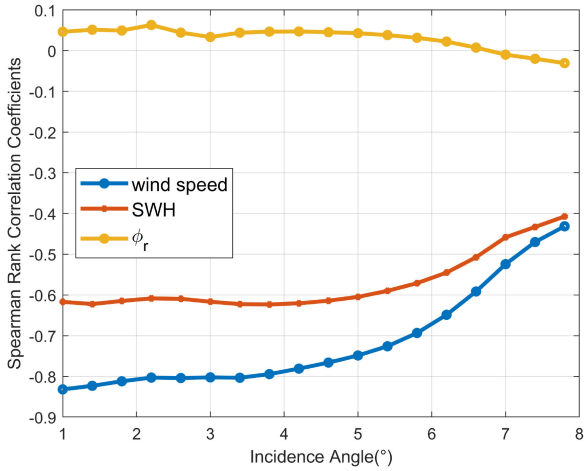

Fig. 5. Spearman rank correlation coefficients between TG2-InIRA σ_0 and wind, SWH.

III. Data Analysis and Model Derivation

A. Data Analysis

The first step of model derivation is to analyze the relationship between the TG2-InIRA measured σ_0 and the parameters related to sea states such as wind speed and SWH. In order to explore the sensitivity of σ_0 on the sea states at small incidence angles, three Spearman rank correlation coefficients are calculated [35], i.e., that between σ_0 and wind speed, that between σ_0 and relative wind direction ϕ_r, and that between σ_0 and SWH. The results are presented in Fig. 5. The relative wind direction ϕ_r is defined as the angle between the wind direction and the incident direction of the radar antenna beam projected on the sea surface, where both directions are measured from true north. If the wind blows toward the projected direction of the radar beam, then ϕ_r is defined as zero.

As can be seen, the σ_0-wind speed correlation coefficients are negative, which is consistent with the quasi-specular reflection theory [36]. As the wind speed increases, the sea surface

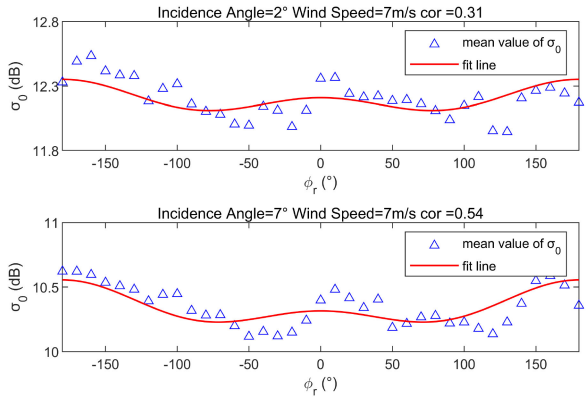

Fig. 6. Relationship between TG2-InIRA σ_0 and ϕ_r at wind speed of 7 m/s and at incidence angles of 2° and 7°. The red solid lines show the curve-fitting results.

becomes rougher and the σ_0 becomes smaller correspondingly. The σ_0-SWH correlation coefficients are also negative as same as the σ_0-wind speed coefficients. The σ_0-ϕ_r coefficients are close to zero, which means the σ_0 is not sensitive to the variation of wind direction. The absolute values of the σ_0-wind speed coefficients are greater than that of the other two, this means that σ_0 is more sensitive to the wind speed than it is sensitive to the wind direction and SWH.

Next, the dependence of σ_0 on wind and SWH is analyzed in detail. The variations of σ_0 versus the relative wind direction at a typical wind speed of 7 m/s and at incidence angles of 2° and 7° are presented in Fig. 6, as shown in which the fluctuations of σ_0 over variation of relative wind direction are quite small and less than 1 dB. As for quantitative comparison, we fit the mean values of the measured σ_0 to a similar model adopted by scatterometer, which are shown as the red curves and calculate the correlation coefficient between σ_0 and the fitted model. It is shown that the correlation coefficient is about 0.54 at 7°, while it is about 0.31 at 2°. It is to say although the relationship between them exhibits a biharmonic behavior, the variations of σ_0 on wind direction are quite small. However, the wind direction is considered in the GMFs of scatterometers because quite larger incidence angles are adopted. As shown in Fig. 8 in [37], the variation of scatterometer σ_0 on wind direction is greater than 5 dB. Chu *et al.* explored the relation of Ku-band σ_0 with wind speed based on TRMM PR, and their results show that the influence of wind direction on σ_0 cannot be neglected if the incidence angle is greater than 13.5° [35]. Based on the above reasons and the maximum incidence angle of TG2-InIRA is 8°, we do not consider the influence of wind direction in this work.

Because the mean value of the collocated SWH is 1.87 m, all available σ_0 are classified into two groups for better demonstrating the SWH influence on σ_0, one group is for SWH $>$ 1.87 m, and the other group is for SWH $\leq$ 1.87 m. Fig. 7 presents the scatter plots of σ_0 variation on wind speed at incidence angles of 1°, 3°, 5°, and 7° in the above two SWH regions. It is clearly shown in Fig. 7 that when the incidence angle increases from 1° to 7°, the variation of σ_0 versus the increase of wind speed becomes smaller. Specifically, taking the SWH $>$ 1.87 m region for example, in the 1° case, the σ_0 decreases about 4 dB as the wind speed increases from 2 to 14 m/s, as shown in Fig. 7(a), while in the 7° case, the σ_0 decreases about 2 dB, as shown in Fig. 7(d). Besides, the decreasing rate of σ_0 under larger SWH is always smaller than that under smaller SWH except for the 7° case. It can be summarized that the σ_0 is much more sensitive to the variation of wind speed under smaller SWH and smaller incidence angle conditions. From the fitted lines, it can be seen that the slope difference between two SWH regions becomes smaller as the incidence angle increases. Fig. 7 also shows that the SWHs are likely larger under larger sea surface wind speeds.

B. Model Derivation

Yan *et al.* [38] analyzed the correlation coefficients between σ_0 and wind speed from near 0° to 18° using the measurements of global precipitation measurement (GPM) Ku/Ka-band dual-frequency precipitation radar (DPR). Their results show that at nadir, the rougher the sea surface, the less the signal can be reflected to radar. Conversely, at incidence angles near 18°, the radar backscatter increases as the sea surface roughness increases. The transition point is around 9.2°, at which the σ_0 loses its dependence on wind speed since the sum of the quasi-specular reflection and the Bragg scattering does not vary along with the surface roughness. It can be inferred that the quasi-specular reflection dominates the backscattering within the incidence range of TG2-InIRA, i.e., 1°–8°, as has also been demonstrated above.

For microwave backscattering from ocean surface at less than 15° incidence angle, the quasi-specular backscattering from an isotropic rough surface meeting the Gaussian statistics can be modeled as following [39]:

$$\sigma_0 = \frac{|R_0|^2}{s}\sec^4\theta \exp\left[-\frac{\tan^2\theta}{s}\right] \tag{2}$$

where $|R_0|^2$ denotes the effective nadir reflection coefficient, s denotes the sea surface mean square slope, and θ denotes the incidence angle.

A lot of efforts have been made to explore the relations of $|R_0|^2$ and s versus wind speed [19], [40], [41]. Freilich *et al.* showed in [21] that $|R_0|^2$ varies between 0.38 and 0.50, while s increases monotonically and nonlinearly as wind speed varies from 0 to 25 m/s for TRMM PR data. Wu suggested that the mean square slope varies approximately as the logarithm of wind speed [42], [43].

For describing the model development process for TG2-InIRA, σ_0 measurements of TG2-InIRA and the modeled σ_0 of (2) are both presented in Fig. 8, as can be clearly seen their variation trends along with wind speed and incidence angle are consistent well. However, there are still some notable differences, especially for smaller and larger wind speeds. It is to say the model of (2) cannot be directly used for wind speed retrieval for TG2-InIRA. The above results inspire us to modify (2) by expressing the effective nadir reflection coefficient $|R_0|^2$ and the mean square slope of sea surface s as functions of wind speed so as to better model the backscattering behavior of TG2-InIRA

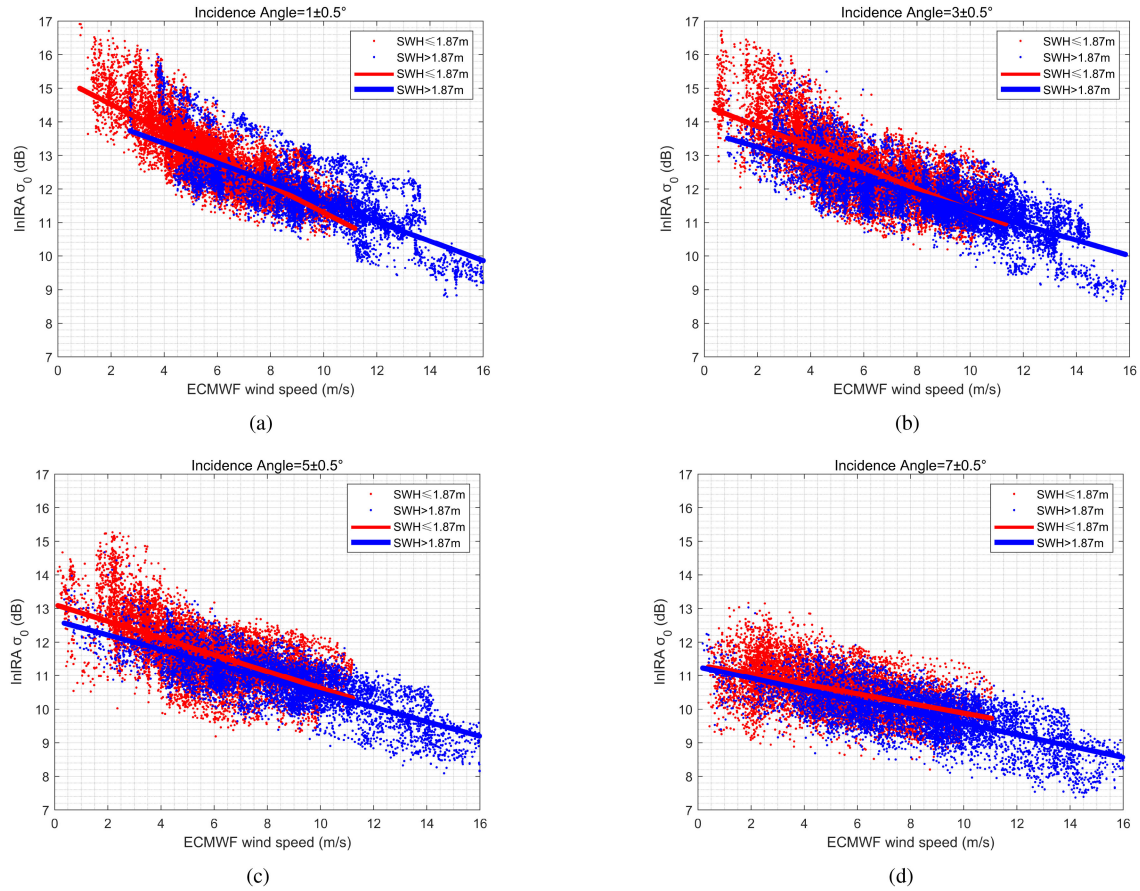

Fig. 7. TG2-InIRA σ_0 variations on wind speed for 1°, 3°, 5° and 7° incidence angles under smaller and larger SWH conditions. The red and blue lines are obtained by linear least square fitting representing SWH $\leq$ 1.87 m and SWH $>$ 1.87 m, respectively.

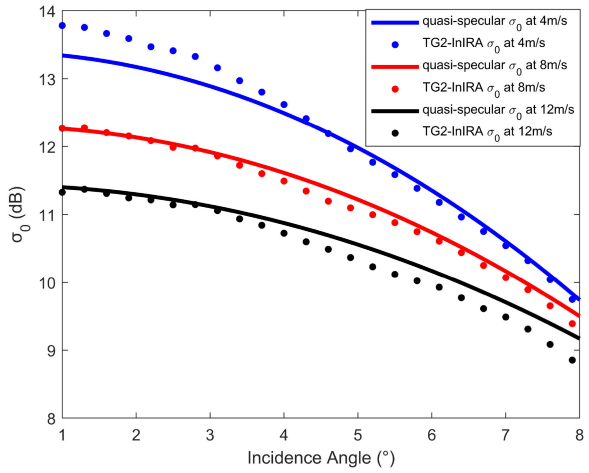

Fig. 8. Comparison between the quasi-specular σ_0 and the mean values of TG2-InIRA σ_0. The scatter plots represent the mean values of TG2-InIRA σ_0 and the lines represent the quasi-specular modeled σ_0.

and then the developed model can be used to retrieve the wind speed.

The modified model is expressed as follows:

$$\sigma_0(\theta, u) = \frac{|R(u)|^2}{s(u)} \sec^4\theta \exp\left[-\frac{\tan^2\theta}{s(u)}\right] \tag{3}$$

where

$$|R(u)|^2 = a_1 u^2 + a_2 u + a_3 \tag{4}$$

$$s(u) = b_1 u^2 + b_2 u + b_3 \tag{5}$$

and u is the wind speed at 10 m above sea surface, θ is the incidence angle, a_1, a_2, a_3, b_1, b_2, and b_3 are the model coefficients obtained by curve fitting.

In this article, we explore the variations of $|R_0|^2$ and s on wind speed and express them as quadratic polynomials by (4) and (5), respectively. The processes for determining a_1, a_2, and a_3 in (4), and b_1, b_2, and b_3 in (5) are outlined as follows. TG2-InIRA measured σ_0 corresponding to incidence angles from 1° to 8°, and the collocated wind speeds from 1.2 to 15.2 m/s are used. The reason why the wind speed range is limited to 15.2 m/s is that the amount of data with wind speeds larger than 15.2 m/s is not enough for fitting the coefficients of the polynomials due to discontinuous observation of TG2-InIRA when in orbit. The concrete fitting steps are as follows.

1) The wind speeds are divided into 71 bins: 1.2 ± 0.5 m/s, 1.4 ± 0.5 m/s, 1.6 ± 0.5 m/s, …, 14.8 ± 0.5 m/s, 15.0 ± 0.5 m/s, 15.2 ± 0.5 m/s.
2) For different wind speed u, $|R(u)|^2$ and $s(u)$ are extracted by fitting (3) using the collocated data.

TABLE I
MODEL COEFFICIENTS OF KULMOD-H

Coefficients	Values	Coefficients	Values
a_1	-0.0026	b_1	-0.000152
a_2	0.0358	b_2	0.0041
a_3	0.3506	b_3	0.0050

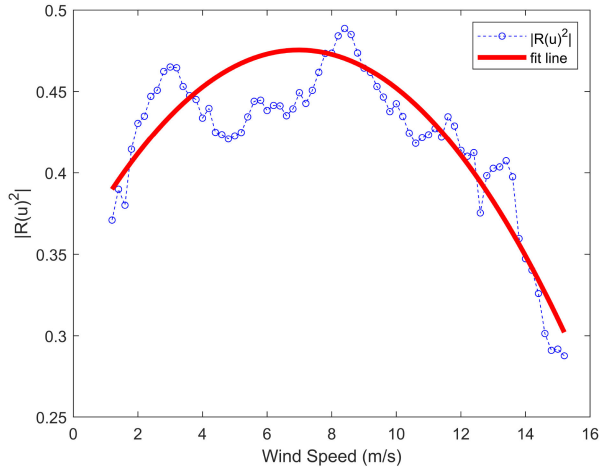

(a)

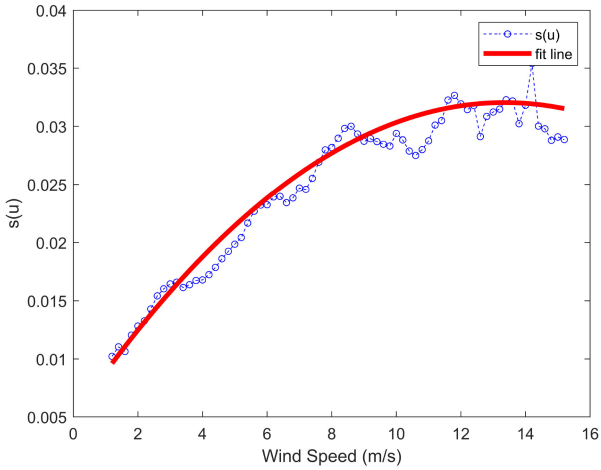

(b)

Fig. 9. Variations of $|R(u)|^2$ and $s(u)$ on wind speed. Small blue circles represent the derived $|R(u)|^2$ and $s(u)$ at step 2) for different wind speeds, while the red lines are from (4) and (5) using the fixed model coefficients.

3) a_1, a_2, and a_3 are obtained by fitting the obtained $|R(u)|^2$ at step 2 to the right-side of (4) using different u; b_1, b_2, and b_3 are obtained by fitting the obtained $s(u)$ at step 2 to the right-side of (5) using different u.

With the above three steps completed, we get all the model coefficients as listed in Table I. Fig. 9(a) and (b) plot the fitted curves of $|R(u)|^2$ and $s(u)$ versus the wind speed u, respectively. Fig. 10 plots the TG2-InIRA σ_0 measurements along with that calculated by the developed KuLMOD-H at different wind speeds versus incidence angles from 1° to 8°. It can be seen that they agree with each other very well. Compared with Fig. 8, the consistency between the measurements and the model values has been obviously improved. In addition, the proposed model results highly agree with the measurements of GPM DPR, as compared with [38, Fig. 5].

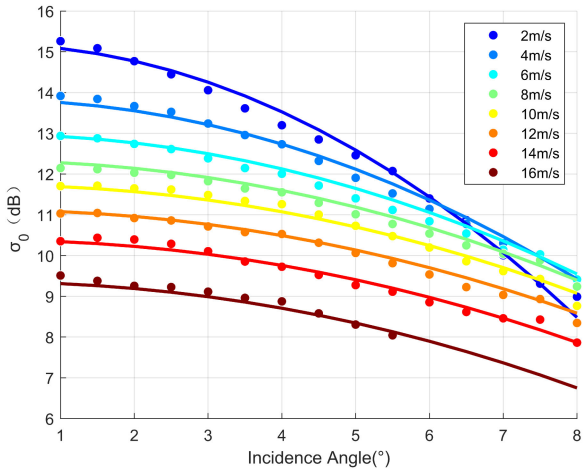

Fig. 10. Comparison of the KuLMOD-H σ_0 and TG2-InIRA σ_0 for incidence angles from 1° to 8°. The solid lines represent the model values while the points represent the mean values of TG2-InIRA σ_0.

IV. METHOD FOR WIND SPEED RETRIEVAL

In 2004, a retrieval algorithm for the application of TRMM PR was proposed by Li based on the maximum likelihood estimation aiming for solving the insensitive problem of σ_0 to wind speed at low incidence angles [27]. Bao *et al.* [28] also proposed a maximum likelihood estimation method based on multiple incidence angles to obtain the optimal wind speed by minimizing the objective function. These methods assumed that σ_0 does not change remarkably, however, although this assumption can ensure retrieval accuracy, there is a cost of spatial resolution reduction.

In our work, if the look-up table approach is directly used to retrieve the wind speed as commonly adopted, the results are not stable when the incidence angles are larger than 4°. This problem can be solved by taking a regularization approach [44], [45]. This is to say, the look-up table approach for incidence angles less than or equal to 4°, and the regularization approach for incidence angles greater than 4°. As shown in Fig. 10, there exists a relatively weaker sensitivity problem of σ_0 on wind speed and even the multisolution problem for larger incidence angles. Based on the assumption that the wind speed should not change much within the swath of TG2-InIRA, we impose the averaged least square wind speed from incidence angles smaller than 4° within the same azimuth angle as the regularization reference for incidence angles larger than 4°. Thus, the regularized wind speed can be obtained using the following objective function:

$$\min \frac{1}{2}|\sigma^0_{\text{measured}}(\theta,u)-\sigma^0_{\text{model}}(\theta,u)|^2+\lambda|u-u_{\text{ref}}|^2 \qquad (6)$$

where u_{ref} is the average of the least square wind speeds for incidence angles smaller than 4° within the same azimuth angle,

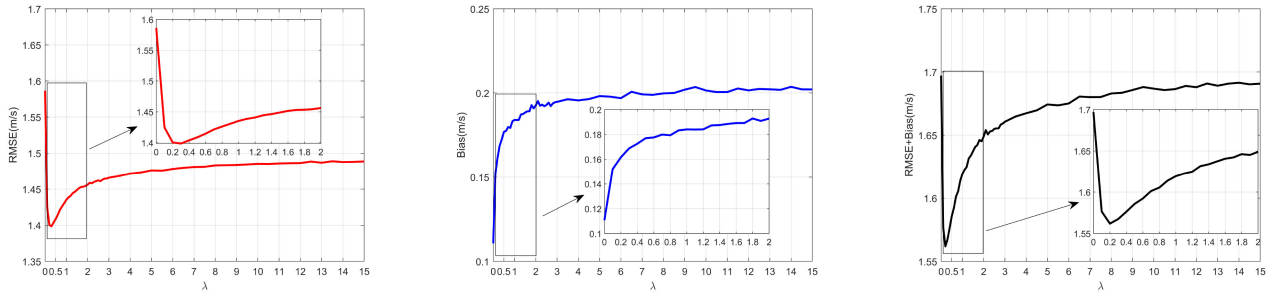

Fig. 11. Retrieved wind speeds as λ varies from 0 to 15, (a)RMSE, (b) bias, and (c) RMSE+bias.

λ is the regularization coefficient, σ^0_{model} is the model value calculated by (3) and $\sigma^0_{\text{measured}}$ is the measured σ_0 by TG2-InIRA.

In order to ensure the robustness of the algorithm, we conduct sufficient experiments to select the optimal λ. It should be noted that in this part of work, we randomly select 10 000 sets of data for guaranteeing both efficiency and reliability at the same time.

We set the range of λ as 0–15, and retrieve the wind speed with different λ. The RMSE, bias, and the sum of RMSE and bias of the retrieved wind speeds are shown in Fig. 11(a)–(c), respectively. As shown in Fig. 11(a), the RMSEs of retrieved wind speeds using regularization are always better than that without regularization (i.e., $\lambda = 0$). As λ increases from 0, the RMSE decreases to a local minimum when it is around 0.3, and then the RMSE increases gradually to a stable level when it is larger than 6. As shown in Fig. 11(b), the bias with regularization is slightly larger than that without regularization. As shown in Fig. 11(c), when λ is equal to 0.2, "Bias + RMSE" has the smallest value. Based on the above results, we finally set $\lambda = 0.2$, because it is able to make a balance between the ambiguity removal and the retrieval accuracy. It is clearly shown that if λ is too smaller, the strength on suppressing the ambiguity is not enough, if it is too larger, the accuracy will be degraded. The proposed regularization approach can not only ensure the accuracy but also maintain the high spatial resolution of wind speed retrieval.

V. Validation and Discussion

In this section, we validate the derived model by three experiments, i.e., the first is to compare the retrieved wind speeds with that from ECMWF-ERA5 alone, the second is to compare the retrieved wind speeds with that from both buoys and ECMWF-ERA5, and the last is to compare the retrieved wind speeds with that from KuLMOD2 [3].

A. Validated by ECMWF Reanalysis Data

We first validate the retrieved results by comparing with the collocated reanalysis wind speeds from ECMWF, and 42941 of the total 171 764 groups of data are used. Fig. 12 compares the wind speeds retrieved from the KuLMOD-H and that from the collocated ECMWF wind speeds, as can be seen from which, they are agreed very well with each other and the RMSE is about

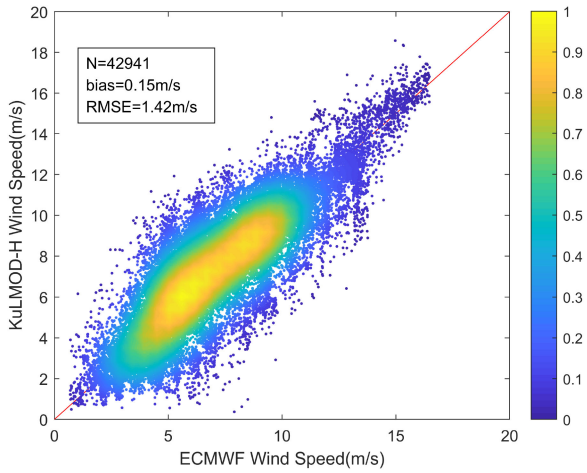

Fig. 12. Density scatter diagram of the retrieved wind speeds using the KuLMOD-H and those collocated from ECMWF. The red line indicates "*y*=*x*" for reference.

1.42 m/s while the mean difference is about 0.15 m/s. It meets the 2 m/s accuracy standard of wind speed measurement [46].

B. Validated by Both Buoy and ECMWF Reanalysis Data

Now, we further validate the retrieved results by comparing both with the *in situ* buoys data and the reanalysis data. Nineteen buoy sets of data have been matched to TG2-InIRA observations. Table II lists the wind speeds retrieved from the KuLMOD-H along with the collocated buoy wind speeds, as can be seen from which, the all groups except for group 2 have differences less than 2 m/s, and especially, 13 of them are less than 1 m/s. The incidence angles of matched measurements cover almost 1° to 8°. The good agreement demonstrates the effectiveness of the developed model as well as the retrieval algorithm. As for the abnormal group 2 with the largest difference of 2.10 m/s, we should investigate if there are some reasons behind it. The corresponding amplitude image and the normalized spectrum image of a small region near the buoy position are presented in Fig. 13(a) and (b), respectively. As it is shown in Fig. 13(a), there are obvious strips along the azimuthal direction, which are generated from ocean waves, and this can be verified by Fig. 13(b), where the wave spectral pattern is clearly shown. It can be inferred that the wave stripes may affect the σ_0 so that

TABLE II
BUOY AND TG2-INIRA COLLOCATED WIND SPEEDS

Group Number	Buoy Stations	UTCTime of Buoy	UTCTime of InIRA	$\theta(^\circ)$	KuLMOD-H Wind Speed(m/s)	Buoy Wind Speed(m/s)	Differences (m/s)
1	51000	201612041230	201612041226	1.07	10.80	10.25	0.55
2	51004	201612051120	201612051124	6.52	5.03	7.13	**-2.10**
3	44014	201612190650	201612190651	5.32	12.22	13.57	-1.35
4	51101	201703151400	201703151404	1.07	4.27	6.01	-1.74
5	51000	201703191140	201703191137	1.16	2.08	4.01	-1.93
6	51000	201704110110	201704110109	1.06	5.86	5.79	0.07
7	51004	201708051830	201708051832	2.45	9.86	10.36	-0.50
8	46059	201712141130	201712141128	2.98	5.16	4.61	0.55
9	46006	201802011220	201802011224	7.95	8.58	8.57	0.01
10	46059	201803141740	201803141745	1.24	4.09	4.84	-0.75
11	46002	201703171450	201703171447	1.03	5.00	4.05	0.95
12	46059	201803171620	201803171624	1.13	6.23	5.73	0.50
13	46059	201806231840	201806231843	4.17	7.57	8.10	-0.53
14	46059	201806261730	201806261727	1.24	8.05	9.78	-1.73
15	51000	201807210930	201807210932	4.69	8.59	7.13	1.46
16	46059	201808181700	201808181657	1.05	9.29	8.91	0.38
17	51004	201811092110	201811092108	1.83	7.24	6.79	0.45
18	46002	201809090520	201809090523	1.16	9.25	9.11	0.14
19	46002	201810191040	201810191037	2.62	5.28	5.40	-0.12

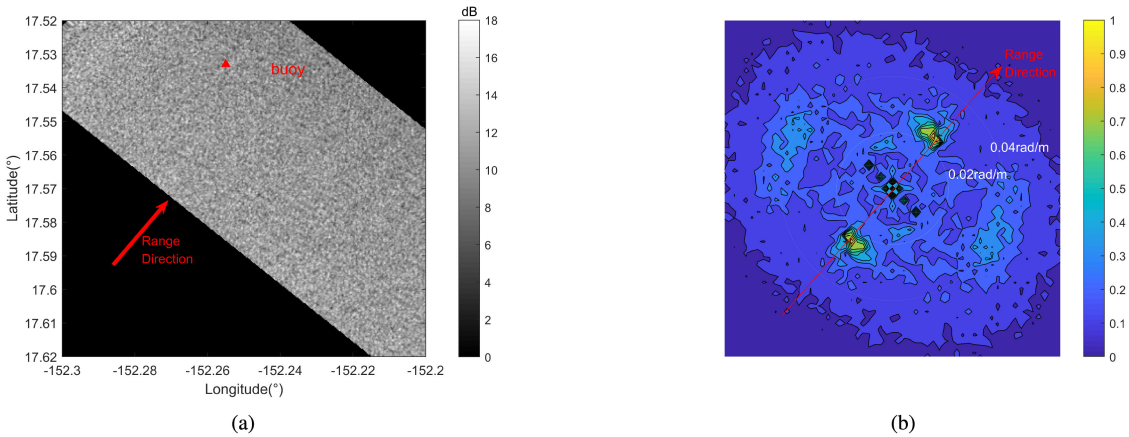

Fig. 13. Collocated data corresponding to the second group data in Table II. (a) Part of the intensity image with buoy position marked. (b) The corresponding image of normalized wave spectral.

the retrieved wind speed has a large error compared with the buoy.

Besides, we double validate the TG2-InIRA results by comparing both with the buoys and the reanalysis data, and present the results in Fig. 14(a), as can be seen, they are highly consistent with each other. We further calculate the difference between the retrieved wind speed and the ERA- 5 reanalysis wind speed, as well as the difference between the retrieved wind speed and the buoy speeds as shown by the red and blue lines in Fig. 14(b), their RMSEs and biases are, respectively, about 1.30 and 0.07 m/s, and about 1.06 and 0.29 m/s. We notice from Fig. 14(b) that the first and 12th groups of data have relatively larger errors between the ERA-5 wind speeds and the retrieved wind speeds, while they are relatively smaller between the buoy wind speeds and the retrieved wind speeds. Considering that the buoy data are from *in situ* measurements while the ERA-5 reanalysis data are obtained through interpolation, so the consistency between the retrieved results and the buoy wind speeds is much more reliable.

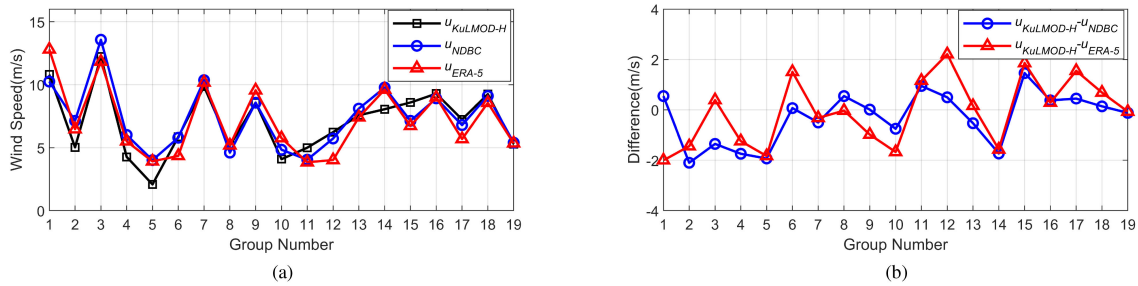

Fig. 14. (a) Triple collocation of TG2-InIRA, NDBC buoy and ERA-5 wind speeds, (b) the wind speed difference between TG2-InIRA and NDBC, and the difference between TG2-InIRA and ERA-5.

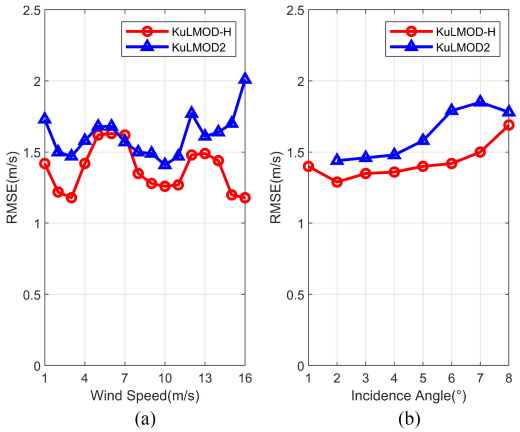

Fig. 15. RMSEs of KuLMOD-H and KuLMOD2 for (a) different wind speeds and (b) different incidence angles.

C. Comparison With the Model KuLMOD2

Compared with the work on KuLMOD2 in [3], we extend the observation data for incidence angles below 2°. Besides, KuLMOD2 is derived by using a simple second-order polynomial obtained based on TRMM PR data, while the proposed model is derived from TG2-InIRA data based on the quasi-specular reflection model.

The same data of Section V-A are used to retrieve the wind speed based on KuLMOD2. The RMSE of the retrieved results is about 1.64 m/s as compared with the ECMWF data. The results are close to the results in [3], where the retrieved wind speeds were compared with that from ASCAT. We further compare the RMSEs of the retrieved wind speeds for different incidence angles and different wind speeds by using the KuLMOD-H and the KuLMOD2 with results presented in Fig. 15, as can be seen from which our new model outperforms the KuLMOD2 obviously.

As Fig. 15(b) shows, the retrieval accuracy decreases as the incidence angle increases, which can be reasonably explained as follows. As shown in Fig. 10, the sensitivity of σ_0 to wind speed decreases as incidence angle increases, and the sensitivity is very crucial for accurate retrieving. It means that the higher the sensitivity, the higher the accuracy can be achieved. In addition, as shown in Fig. 6, the correlation between σ_0 and wind direction increases as incidence angle increases, it means at larger incidence angles, the σ_0 measurement is likely influenced by wind direction and thus the retrieval accuracy is likely influenced. This influence deserves us to take into account in our future work for further improving the retrieval accuracy of wind speed.

The above three experiments validate the developed model and the retrieval algorithm very well. It makes us confident about their applicability. We should point out that, the results for wind speeds greater than 15 m/s are only preliminarily validated with good accuracy by the collocated data of ECMWF because the available datasets are limited.

VI. Conclusion

In this article, the variations of TG2-InIRA σ_0 on wind speed, wind direction, and SWH are first demonstrated and analyzed, then a high-resolution GMF named as KuLMOD-H is developed based on the quasi-specular reflection model. The key to the model derivation is to expand the effective nadir reflection coefficient and the sea surface mean square slope as quadratic polynomials of wind speed. As for the retrieval stage, the regularization approach combined with the look-up table approach is adopted for accurate retrieval of wind speed at all incidence angles for TG2-InIRA. The retrieved results are well validated by both the collocated ECWMF reanalysis data and the buoy data. Besides, it is shown that the performance of KuLMOD-H surpasses the KuLMOD2.

As it is demonstrated, TG2-InIRA σ_0 is also influenced by SWH at low incidence angles. It deserves further exploration for the possibility of retrieving SWH along with the wind speed at the same time or to exclude the influence of which for achieving much higher accuracy of wind speed retrieval.

Acknowledgment

The authors would like to thank the European Centre for Medium-Range Weather Forecasts for the straightforward and rapid electronic access to the ERA-5 reanalysis data. The authors would also like to thank the American NDBC for providing the buoy data. The authors would also like to thank the anonymous reviewers for their pertinent comments and constructive suggestions for improving the presentation of this work.

References

[1] J. Yang, L. Ren, and G. Zheng, "The first quantitative remote sensing of ocean by Tiangong-2 interferometric imaging altimeter," *Acta Oceanologica Sinica*, vol. 39, no. 2, pp. 129–130, 2017.

[2] Y. Zhang *et al.*, "Interferometric imaging radar altimeter on board chinese Tiangong-2 space laboratory," in *Proc. Asia-Pacific Microw. Conf.*, 2018, pp. 851–853.

[3] L. Ren, J. Yang, Y. Jia, X. Dong, J. Wang, and G. Zheng, "Sea surface wind speed retrieval and validation of the interferometric imaging radar altimeter aboard the Chinese Tiangong-2 space laboratory," *IEEE J. Sel. Topics Appl. Earth Observ. Remote Sens.*, vol. 11, no. 12, pp. 4718–4724, Dec. 2018.

[4] L. Ren, J. Yang, X. Dong, Y. Jia, and Y. Zhang, "Preliminary significant wave height retrieval from interferometric imaging radar altimeter aboard the Chinese Tiangong-2 space laboratory," *Remote Sens.*, vol. 13, no. 12, 2021, Art. no. 2413.

[5] L. Ren, J. Yang, X. Dong, Y. Zhang, and Y. Jia, "Preliminary evaluation and correction of sea surface height from Chinese Tiangong-2 interferometric imaging radar altimeter," *Remote Sens.*, vol. 12, no. 15, 2020, Art. no. 2496.

[6] X. Dong, Y. Zhang, and W. Zhai, "Design and algorithms of the Tiangong-2 interferometric imaging radar altimeter processor," in *Proc. Prog. Electromagn. Res. Symp.–Spring*, 2017, pp. 3802–3803.

[7] D. B. Chelton, M. H. Freilich, J. M. Sienkiewicz, and J. M. V. Ahn, "On the use of QuikSCAT scatterometer measurements of surface winds for marine weather prediction," *Monthly Weather Rev.*, vol. 134, no. 8, pp. 2055–2071, 2006.

[8] G. Zhang, W. Perrie, X. Li, and J. A. Zhang, "A hurricane morphology and sea surface wind vector estimation model based on C-band cross-polarization SAR imagery," *IEEE Trans. Geosci. Remote Sens.*, vol. 55, no. 3, pp. 1743–1751, Mar. 2017.

[9] D. B. Chelton and P. J. McCabe, "A review of satellite altimeter measurement of sea surface wind speed: With a proposed new algorithm," *J. Geophys. Res.*, vol. 90, no. C3, 1985, Art. no. 4707.

[10] F. M. Monaldo, D. R. Thompson, R. C. Beal, W. G. Pichel, and P. Clemente-Colon, "Comparison of SAR-derived wind speed with model predictions and ocean buoy measurements," *IEEE Trans. Geosci. Remote Sens.*, vol. 39, no. 12, pp. 2587–2600, Dec. 2001.

[11] A. Stoffelen and D. Anderson, "Scatterometer data interpretation: Estimation and validation of the transfer function CMOD4," *J. Geophys. Res., Oceans*, vol. 102, no. C3, pp. 5767–5780, 1997.

[12] H. Hersbach, A. Stoffelen, and S. de Haan, "An improved C-band scatterometer ocean geophysical model function: CMOD5," *J. Geophysical Res.*, vol. 112, no. C3, 2007, Art. no. C03006.

[13] H. Hersbach, "Comparison of C-band scatterometer CMOD5.N equivalent neutral winds with ECMWF," *J. Atmos. Ocean. Technol.*, vol. 27, no. 4, pp. 721–736, 2010.

[14] P. W. Vachon and J. Wolfe, "C-band cross-polarization wind speed retrieval," *IEEE Geosci. Remote Sens. Lett.*, vol. 8, no. 3, pp. 456–459, May 2011.

[15] S. Yueh, R. West, F. Li, W.-Y. Tsai, and R. Lay, "Dual-polarized Ku-band backscatter signatures of hurricane ocean winds," *IEEE Trans. Geosci. Remote Sens.*, vol. 38, no. 1, pp. 73–88, Jan. 2000.

[16] A. Bentamy, S. A. Grodsky, J. A. Carton, D. Croizã-Fillon, and B. Chapron, "Matching ASCAT and Quikscat winds," *J. Geophys. Res. Oceans*, vol. 117, no. C2, 2012, Art. no. C02011.

[17] L. Ricciardulli and F. J. Wentz, "A scatterometer geophysical model function for climate-quality winds: QuikSCAT Ku-2011," *J. Atmos. Ocean. Technol.*, vol. 32, 2014, Art. no. 150904131243002.

[18] X. Yang, X. Li, W. G. Pichel, and Z. Li, "Comparison of ocean surface winds from ENVISAT ASAR, MetOp ASCAT Scatterometer, Buoy Measurements, and NOGAPS Model," *IEEE Trans. Geosci. Remote Sens.*, vol. 49, no. 12, pp. 4743–4750, Dec. 2011.

[19] W. Shao, X. M. Li, S. Lehner, and C. Guan, "Development of polarization ratio model for sea surface wind field retrieval from TerraSAR-X HH polarization data," *Int. J. Remote Sens.*, vol. 35, no. 11/12, pp. 4046–4063, 2014.

[20] J. Horstmann, H. Schiller, J. Schulz-Stellenfleth, and S. Lehner, "Global wind speed retrieval from SAR," *IEEE Trans. Geosci. Remote Sens.*, vol. 41, no. 10, pp. 2277–2286, Oct. 2003.

[21] M. H. Freilich and B. A. Vanhoff, "The relationship between winds, surface roughness, and radar backscatter at low incidence angles from TRMM precipitation radar measurements," *J. Atmos. Ocean. Technol.*, vol. 20, pp. 549–562, 2003.

[22] L. Ren, J. Yang, G. Zheng, and J. Wang, "A Ku-band low incidence model for wind speed retrieval from TRMM precipitation radar data," in *Proc. 9th Int. Symp. Multispectral Image Process. Pattern Recognit.*, J. Liu and H. Sun, Eds., Enshi, China, 2015, Art. no. 981514.

[23] N. Tran, B. Chapron, and D. Vandemark, "Effect of long waves on Ku-band ocean radar backscatter at low incidence angles using TRMM and altimeter data," *IEEE Geosci. Remote Sens. Lett.*, vol. 4, no. 4, pp. 542–546, Oct. 2007.

[24] V. Hesany, W. Plant, and W. Keller, "The normalized radar cross section of the sea at 10 incidence," *IEEE Trans. Geosci. Remote Sens.*, vol. 38, no. 1, pp. 64–72, Jan. 2000.

[25] T. Kozu *et al.*, "Development of precipitation radar onboard the tropical rainfall measuring mission (TRMM) satellite," *IEEE Trans. Geosci. Remote Sens.*, vol. 39, no. 1, pp. 102–116, Jan. 2001.

[26] X. Chu, Y. He, and G. Chen, "Asymmetry and anisotropy of microwave backscatter at low incidence angles," *IEEE Trans. Geosci. Remote Sens.*, vol. 50, no. 10, pp. 4014–4024, Oct. 2012.

[27] L. Li, E. Im, L. N. Connor, and P. S. Chang, "Retrieving ocean surface wind speed from the TRMM Precipitation Radar measurements," *IEEE Trans. Geosci. Remote Sens.*, vol. 42, no. 6, pp. 1271–1282, Jun. 2004.

[28] Q. Bao, Y. Zhang, S. Lang, M. Lin, and P. Gong, "Sea surface wind speed inversion using the low incident NRCS measured by TRMM precipitation radar," *IEEE J. Sel. Topics Appl. Earth Observ. Remote Sens.*, vol. 9, no. 11, pp. 5262–5271, Nov. 2016.

[29] X. Chu, Y. He, and G. Chen, "A new algorithm for wind speed at low incidence angles using TRMM Precipitation Radar data," in *Proc. IEEE Int. Geosci. Remote Sens. Symp.*, 2010, pp. 4162–4165.

[30] Y. Zhang, Q. Bao, M. Lin, and S. Lang, "Wind speed inversion and in-orbit assessment of the imaging altimeter on Tiangong-2 space station," *Acta Oceanologica Sinica*, vol. 39, no. 12, pp. 114–120, 2020.

[31] L. Ren, J. Yang, G. Zheng, and J. Wang, "Wind speed retrieval from Ku-band Tropical Rainfall Mapping Mission precipitation radar data at low incidence angles," *J. Appl. Remote Sens.*, vol. 10, no. 1, 2016, Art. no. 016012.

[32] P. Gaspar, F. Ogor, P.-Y. Le Traon, and O.-Z. Zanife, "Estimating the sea state bias of the TOPEX and POSEIDON altimeters from crossover differences," *J. Geophys. Res.*, vol. 99, no. C12, 1994, Art. no. 24981.

[33] D. B. Chelton, "The sea state bias in altimeter estimates of sea level from collinear analysis of TOPEX data," *J. Geophys. Res.*, vol. 99, no. C12, 1994, Art. no. 24995.

[34] B. R. Thomas, E. C. Kent, and V. R. Swail, "Methods to homogenize wind speeds from ships and buoys," *Int. J. Climatol.*, vol. 25, no. 7, pp. 979–995, 2005.

[35] X. Chu, Y. He, and V. Y. Karaev, "Relationships between Ku-band radar backscatter and integrated wind and wave parameters at low incidence angles," *IEEE Trans. Geosci. Remote Sens.*, vol. 50, no. 11, pp. 4599–4609, Nov. 2012.

[36] D. Barrick, "Wind dependence of quasi-specular microwave sea scatter," *IEEE Trans. Antennas Propag.*, vol. 22, no. 1, pp. 135–136, Jan. 1974.

[37] M. A. Donelan and W. J. Pierson, "Radar scattering and equilibrium ranges in wind-generated waves with application to scatterometry," *J. Geophys. Res.*, vol. 92, no. C5, 1987, Art. no. 4971.

[38] Q. Yan, J. Zhang, C. Fan, and J. Meng, "Analysis of Ku- and Ka-band sea surface backscattering characteristics at low-incidence angles based on the GPM dual-frequency precipitation radar measurements," *Remote Sens.*, vol. 11, no. 7, pp. 754–775, 2019.

[39] G. R. Valenzuela, "Theories for the interaction of electromagnetic and oceanic waves - A review," *Boundary-Layer Meteorol.*, vol. 13, no. 1–4, pp. 61–85, 1978.

[40] X. Li, Y. He, B. Zhang, J. Ge, and X. Chu, "A geometrical optics model based on the non-Gaussian probability density distribution of sea surface slopes for wind speed retrieval at low incidence angles," *Int. J. Remote Sens.*, vol. 37, no. 3, pp. 537–550, 2016.

[41] S. Li, D. Zhao, L. Zhou, and B. Liu, "Dependence of mean square slope on wave state and its application in altimeter wind speed retrieval," *Int. J. Remote Sens.*, vol. 34, no. 1, pp. 264–275, 2013.

[42] J. Wu, "Sea-surface slope and equilibrium wind-wave spectra," *Phys. Fluids*, vol. 15, no. 5, pp. 741–747, 1972.

[43] W. Jin, "Mean square slopes of the wind-disturbed water surface, their magnitude, directionality, and composition," *Radio Sci.*, vol. 25, no. 1, pp. 37–48, 1990.

[44] A. B. Bakushinskii, "A general method of constructing regularizing algorithms for a linear incorrect equation in Hilbert space," *USSR Comput. Math. Math. Phys.*, vol. 7, no. 3, pp. 279–287, 1967.

[45] R. A. Polyak, "Regularized Newton method for unconstrained convex optimization," *Math. Program.*, vol. 120, no. 1, pp. 125–145, 2009.

[46] F. Monaldo, C. Jackson, X. Li, and W. G. Pichel, "Preliminary evaluation of Sentinel-1 A wind speed retrievals," *IEEE J. Sel. Top. Appl. Earth Observ. Remote Sens.*, vol. 9, no. 6, pp. 2638–2642, Jun. 2016.

Guo Li received the B.S. degree in communication engineering from the Ocean University of China, Tsingtao, China, in 2017. She is currently working toward the Ph.D. degree in electromagnetic and microwave technology with the National Space Science Center, Chinese Academy of Sciences, Beijing, China.

Her research interest includes the inversion of ocean surface wind and wave parameters based on InIRA images.

Yunhua Zhang (Member, IEEE) received the B.S. degree in electrical engineering from Xidian University, Xi'an, China, in 1989, and the M.S. and Ph.D. degrees in electrical engineering from Zhejiang University, Hangzhou, China, in 1993 and 1995, respectively.

He is currently a Professor with the National Space Science Center, Chinese Academy of Sciences, Beijing, China, and the Director of the CAS Key Laboratory of Microwave Remote Sensing. He is also a Professor with the School of Electronic, Electrical, and Communication Engineering, University of Chinese Academy of Sciences, Beijing, where he lectured the modern radar theory and technology to the postgraduate students. His research interests include the system design and signal processing of microwave sensors (high-resolution radar, interferometric radar, radar altimeter, and noise radar), polarimetric radar target decomposition, application of compressive sensing in radar, and antennas and computational electromagnetics.

Dr. Zhang is the Chief Designer for the Chinese Tiangong-2 Interferometric Imaging Altimeter, which is the first spaceborne wide-swath radar altimeter launched in September 15, 2016.

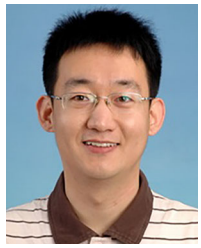

Xiao Dong (Member, IEEE) received the B.S. degree in electrical engineering from Xidian University, Xi'an, China, in 2009, and the Ph.D. degree in electrical engineering from the University of Chinese Academy of Sciences, Beijing, China, in 2015, respectively.

He is currently an Associate Professor with National Space Science Center, Chinese Academy of Sciences, Beijing, China. His research interests include signal processing and radar imaging.